Ocean Engineering 109 (2015) 83–92

Contents lists available at ScienceDirect

Ocean Engineering

journal homepage: www.elsevier.com/locate/oceaneng

An effective CFD approach for marine-vehicle maneuvering simulation based on the hybrid reference frames method

Wu Xiaocui[a], Wang Yiwei[a], Huang Chenguang[a], Hu Zhiqiang[b], Yi Ruiwen[b]

[a] Key Laboratory for Mechanics in Fluid Solid Coupling Systems, Institute of Mechanics, Chinese Academy of Sciences, Beijing, China
[b] State Key Laboratory of Robotics, Shenyang Institute of Automation, Chinese Academy of Sciences, Shenyang, Liaoning, China

ARTICLE INFO

Article history:
Received 25 July 2014
Accepted 26 August 2015
Available online 24 September 2015

Keywords:
Maneuvering characteristics
Hybrid reference frames method
Rotating arm test
SUBOFF model

ABSTRACT

The computational efficiency of CFD on maneuverability simulation poses a great difficulty resulting in its restricted applications. A hybrid reference frames method is established that combines the rotating reference frame method and an added momentum source method. The computational domain is separated into two parts under the rotating reference frame and the inertial frame respectively. A single mesh is needed for all conditions of a testing model such as different rotating arm radius, pitch angles and drift angles. The validation is carried out based on the numerical simulations on the flow fields around the SUBOFF models including sterns and full appended models. Results show that the stability derivatives of the yawing moment and yawing force agree well with the experimental data. Using a dimensional analysis method, the influences of the rotating arm radius and linear velocity are investigated. The similarity is maintained when the radius is constant, and the rotating effect performs strongly when the radius is small. The effects of pitch angle and drift angle are also discussed when the linear velocity is fixed with the fully appended SUBOFF model.

1. Introduction

As one of the most important performance characteristics of marine vehicles, maneuvering is the foundation of navigation safety and effective service. The main objectives of maneuvering simulation are to obtain the hydrodynamic forces under various control conditions, to evaluate the effect on maneuvering and operational limitations of configuration changes (Mackay, 1999), to gain and minimize the consequences of extreme motions (Watt and Bohlmann, 2004), and to advise operators. Various tools are available to provide a predictive capability. Free-swimming scale models are considered to be one of the best predictors of full-scale maneuvering (Hess et al., 2004). The rotating arm pool and the planar motion mechanism (PMM) are also common experiment methods for small scale models. However, these tests have high costs, and it is difficult to obtain full similarity in the experimental facility.

With the development of computer technology, the computational fluid dynamics (CFD) method has been applied to a variety of problems in the field of aircraft and ship design. Most studies focus on the simulation of wind and water tunnels (Williams et al., 2002; Watt et al., 1993), including a computation of positional derivatives (Kim et al., 2001), an extraction of control derivatives (Arabshahi and Gibeling, 2000), and a study of propeller-hull-rudder interaction (Simonsen and Stern, 2005).

Using this method, hydrodynamic coefficients can also be obtained by constructing different running conditions. The simulation of the maneuvering characteristics (Mackay, 2009) is based on the standard submarine six degree-of-freedom (DOF) equations of motion described by Gertler and Hagen (1967), which have been revised by Feldman (1979).

Gregory et al. (2004) put a deformed body in rectilinear flow to investigate the flow separation over a body of revolution in steady turn. This method may have difficulties with model construction and grid generation for a vehicle with many appendages or a complex geometry. A dynamic mesh based CFD method, such as overset, is widely used to perform unsteady maneuvering simulations. Racine and Paterson (2005) successfully computed all stability derivatives and eleven significant maneuvering coefficients for a marine vehicle using an overset grid method. Unfortunately, the computation cost is prodigious. Additionally, using an overlapping grid system, Orihara and Miyata (2003) evaluated the added resistance of ships in regular incident waves. Suzuki et al. (2007) simulated the motion of an underwater vehicle with mechanical pectoral fins. To avoid the great demand of computational resources, Hu et al. (2007) completed calculations of the hydrodynamic forces and moments for an autonomous underwater vehicle (AUV) in a rotating frame of reference. Hu and Lin (2008) derived the governing equations in the rotating reference

E-mail address: wangyw@imech.ac.cn (Y. Wang).

http://dx.doi.org/10.1016/j.oceaneng.2015.08.057
0029-8018/

frame to obtain the formula of added momentum sources. The hydrodynamic coefficients for an autonomous underwater vehicle (AUV) were calculated using the CFD method with added momentum sources. Zhang et al. (2013) used the added momentum sources method and a novel hybrid meshing scheme to simulate the flow over a series of axisymmetric submarine hulls in steady turning condition. The CFD results agreed with the experimental data of the SUBOFF model. Detailed SUBOFF model results for surface skin friction lines, flow separation, leeside vortex development, longitudinal lateral force distributions, and total forces and moments on the body are described. The meshes were reconstructed in each condition in their work to ensure the grid and lateral boundaries are aligned with the flow field, which are labor intensive if a complete set of maneuvering simulations for a vehicle is carried out.

The objective of this work is to develop a more effective method for computing hydrodynamic coefficients of underwater vehicles with the hybrid reference frames method. The Navier–Stokes (NS) equations in the hybrid reference frames are adopted as the governing equations. The rotating relative frame is used in the core region with a new formation of the source momentum, while the absolute frame is used in the other region. In the present method, one mesh is needed for all working conditions of a vehicle, such as pitch angle, drift angle, and rotating arm tank radius. The maneuvering of the SUBOFF model (Roddy, 1990) is simulated using the hybrid reference frames method, and numerical results agree with the experimental data. The influences of the rotating radius and velocity are further investigated.

2. Mathematical models

2.1. The Navier–Stokes equations in a body-fixed frame

Due to the rotating movement of the underwater vehicle, the Coriolis acceleration is involved in the equation. If the reference frame is built on the vehicle, the vehicle will be at rest relatively all of the time; thus, the standard NS equation must be modified accordingly due to the difference between an absolute frame and a relative one.

The NS equation in a body fixed frame of reference Hu and Lin (2008) is expressed as follows:

$$\rho\frac{dU}{dt} = \rho f + \nabla\cdot\left(-p\delta + \mu\left(\nabla U + \frac{1}{3}(\nabla U)^T\right)\right) - \rho a_e - \rho a_c \tag{1}$$

where ρ is the density of the fluid, t is the time variable, $U$is the absolute velocity of the fluid, f is the body force of unit mass of fluid, p is the pressure; μ is the dynamic viscosity, δ is the identity matrix, ∇ represents the Hamilton operator, and the superscript T denotes transpose of a matrix, $a_e$is the acceleration of entrainment, and a_c is the Coriolis acceleration.

In the absolute and inertial reference frame, the NS equation can be written as:

$$\rho\frac{dU}{dt} = \rho f + \nabla\cdot\left(-p\delta + \mu\left(\nabla U + \frac{1}{3}(\nabla U)^T\right)\right) \tag{2}$$

Thus, the added momentum source in a body fixed frame of reference is Eq. (1) minus Eq. (2):

$$MS = -\rho a_e - \rho a_c = -\rho\left(\dot{V} + \dot{\Omega}\times r + \Omega\times(\Omega\times r) + \Omega\times V\right) - 2\rho(\Omega\times U_r) \tag{3}$$

where $V$and $\Omega$is the linear velocity and angular velocity of the vehicle, respectively, U_r is the relative velocity, $r$is the relative position vector, and a superscript dot is used to denote derivatives with respect to t.

2.2. The NS equation in a rotating frame of reference

Single Rotating Reference Frames (SRFs) and Multiple Rotating Reference Frames (MRFs) are commonly used to solve the rotating motion in the CFD method. The NS equation in a rotating frame of reference can be written as:

$$\rho\frac{dU}{dt} = \rho f + \nabla\cdot\left(-p\delta + \mu\left(\nabla U + \frac{1}{3}(\nabla U)^T\right)\right) - \rho\left(2\Omega\times U_r + \Omega\times(\Omega\times r)\right) \tag{4}$$

Compared with the NS equation in an inertial frame, the added momentum sources in the rotating frame of reference can be calculated from Eq. (4) minus Eq. (2):

$$MS' = -\rho\left(2\Omega\times U_r + \Omega\times(\Omega\times r)\right) \tag{5}$$

In the condition of the rotating arm test, the linear velocity of the vehicle V, angular velocity $\Omega = const$, Eq. (3) becomes the same as Eq. (5). Thus, the SRF (MRF) method is equivalent to the body-fixed frame method. So the SRF (MRF) method can be used to simulate the rotating arm tank of vehicle instead of the body-fixed frame method.

2.3. The hybrid reference frames method

In SRF (MRF), a rotating arm tank domain is built (as shown in Fig. 1). Point A is the center of rotation, Point B is the moment center, Ω is the angle velocity of the vehicle, and R_0 is the radius of the rotating arm tank. Fig. 2 shows the computational domain, which is separated into two parts. The rotating reference frame is adopted in the circle part and an inertial frame is set in the other. If the model runs with a non-zero pitch angle or drift angle, the flow direction can be non-parallel with the domain boundary. The rotating radius or speed can be set by altering the value of the

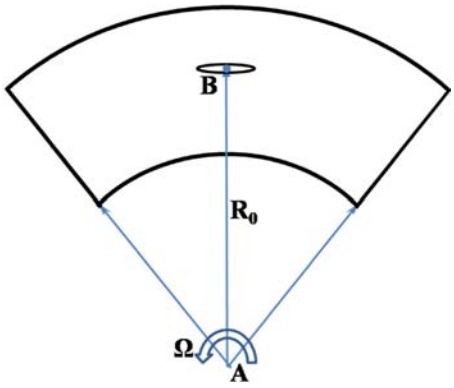

Fig. 1. A rotating frame of reference method domain for simulation of rotating arm tank.

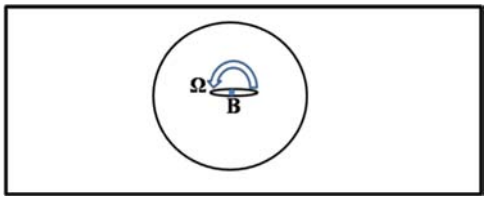

Fig. 2. A semi-relative reference frame method domain for simulation of rotating arm.

moment source. As a result, the mesh can be used in all working conditions for an underwater vehicle in the present method.

In Fig. 1, the rotation center is the point A, and the added momentum sources can be written component by component, viz.

$$\begin{aligned} MS_{xA} &= -\rho\left(\Omega\times\left(\Omega\times(x-x_A)\right)+2\Omega\times U_r\right)\\ MS_{yA} &= -\rho\left(\Omega\times\left(\Omega\times(y-y_A)\right)+2\Omega\times U_r\right)\\ MS_{zA} &= -\rho\left(\Omega\times\left(\Omega\times(z-z_A)\right)+2\Omega\times U_r\right) \end{aligned} \tag{6}$$

In Fig. 2, the rotation center is the point B, and the added momentum sources can be written component by component, viz.

$$\begin{aligned} MS_{xB} &= -\rho\left(\Omega\times\left(\Omega\times(x-x_B)\right)+2\Omega\times U_r\right)\\ MS_{yB} &= -\rho\left(\Omega\times\left(\Omega\times(y-y_B)\right)+2\Omega\times U_r\right)\\ MS_{zB} &= -\rho\left(\Omega\times\left(\Omega\times(z-z_B)\right)+2\Omega\times U_r\right) \end{aligned} \tag{7}$$

where (x, y, z) is the any point coordinate in domain, (x_A, y_A, z_A) is the A point coordinate, (x_B, y_B, z_B) is the B point coordinate, and the rotation axis is Z. Because A and B are in the coaxial position, $x_B = x_A$, $|y_B - y_A| = R_0$, $z_B = z_A$.

With the coordinate transformation of the rotation center from the rotating arm tank (A) to the momentum center of the underwater vehicle (B), the added momentum source in the rotating reference frame part (the circle part in Fig. 2) becomes:

$$\Delta = \left(MS_y\right)_A - \left(MS_y\right)_B = -\rho\Omega\times\left(\Omega\times R_0\right) \tag{8}$$

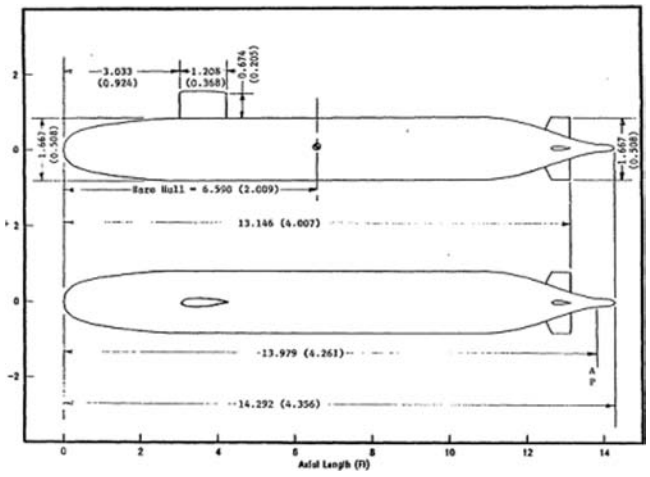

Fig. 3. Drawing of the SUBOFF model.

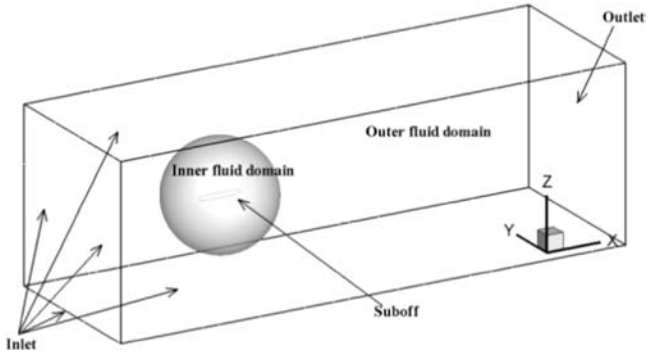

Fig. 4. A computational domain in semi-relative reference frame method.

3. Numerical methods

3.1. Physical model for the testing case

The SUBOFF model is computed with the new method, for which experimental results are from Roddy's report (Roddy, 1990). The SUBOFF project was developed by Submarine Technology Program Office of the Defense Advanced Research Projects Agency to evaluate various flow field predictions for an axisymmetric hull, both with and without appendages (Groves et al., 1989). The project was intended to compare the predictions with model experimental data and to develop methods that could be used in the design of future advanced submarines (Huang et al., 1989).

The geometric characteristics of the SUBOFF model (Groves et al., 1989) are given in Fig. 3. The overall length of the model is L=4.356 m, while the length between perpendiculars (the characteristic length used for nondimensionalization of the hydrodynamic forces and moments) is 4.261 m. The maximum diameter is 0.508 m.

3.2. Computational domain

The computational domain can be set up as a cube, which is separated into two parts (as shown in Fig. 4). The rotating reference frame is adopted in the sphere part, and the center of the sphere must be the moment center of the model. The radius of the sphere is twice the body length. The added momentum source in the sphere part is calculated with Eq. (8). The inertial frame is set in the other part.

The computational domain is discretized into a hybrid unstructured mesh (as shown in Fig. 5), including tetrahedral and prism cells. The region around the model is refined and the

Table 1
A comparison of direct resistance of the SUBOFF with sterns model.

V (Kn)	Computational values (N)			Experimental value (N) (Huang et al.,1989)
	Coarse mesh (2.79 million cells)	Medium mesh (4.53 million cells)	Fine mesh (11.64 million cells)	
5.92	110.75	107.11	107.46	95.41
11.85	380.55	364.13	363.89	361.80
17.78	811.45	770.47	769.41	765.90

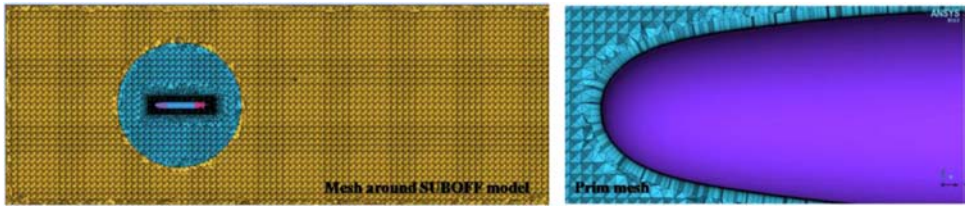

Fig. 5. Computational mesh.

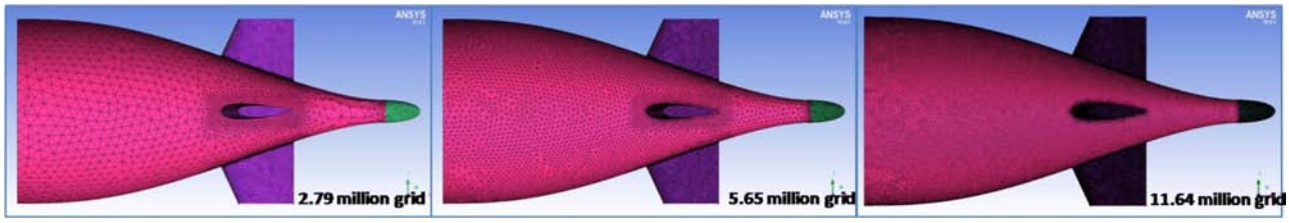

Fig. 6. Surface meshes of the three sets of grids used for grid-independence investigation.

maximum Y^+ value around the model surface is 4 by the usage of the prism cells.

Steady numerical simulations are performed based on finite-volume method with the SIMPLE scheme by using commercial CFD software ANSYS Fluent. The Multiple Rotating Reference Frames (MRF) method is adopted, and additional momentum sources are set by using User-Defined Functions (UDFs). The equations are discretized by a second order upwind differencing scheme in space. The second order scheme was selected for pressure interpolation and the least squares cell based option is used for gradient calculation. The SST $k-\omega$ model is adopted to simulate the turbulent flow (Wilcox, 2001).

The velocity condition is applied to the inlet, and remaining boundaries are fixed as zero average static pressure outlets. The experimental values that the fluid in the domain is water at 18 °C, with $\rho = 998.55kg/m^3$ and $\mu = 0.001053kg/(m{\cdot}s)$ from experimental values (Roddy, 1990). The pressure of reference is set to 1 atm.

3.3. Grid sensitivity investcation

To investigate the sensitivity of the results to the grid resolution, three sets of grids are used with 2.79, 4.53 and 11.64 million nodes respectively (as shown in Fig. 6). The grid densities on the surface vary while the heights of the boundary layer prim cells are fixed among the meshes.

A comparison of direct resistance of the SUBOFF with sterns model is shown in Table 1. The inlet velocities of various cases are at 5.92, 11.85 and 17.78 Knot respectively. It is indicated that the differences can be neglected between the medium and fine meshes s and the computation values of resistance are in good agreement with the experimental values. Thus, the medium mesh with about 4.53 million cells is selected as the final grid.

4. Validation of the numerical approach

4.1. Simulations with the SUBOFF-sterns model

4.1.1. Results for various angle velocities

Maneuvering simulations with various angle velocities are firstly performed to verify the calculation reliability of the present approach. The SUBOFF with sterns model is simulated in a rotating condition using the hybrid reference frames method introduced above, which the radius of the rotating arm tank is 18 m, and the angle velocity varies from 0.08 to 2.22 rad/s. Fig. 7 shows that the yawing force and yawing moment vary with the angle velocity, and the computational values are in fairly good agreement with the experimental results (Roddy, 1990).

The stability derivatives by fitting values from computational results are listed in Table 2, which are also compared with the experiment results. The stability derivative of yawing force is calculated by $Y'_r = \frac{Y/\Omega}{0.5\rho VL^3}$, while the stability derivative of yawing moment. $N'_r = \frac{N/\Omega}{0.5\rho VL^4}$. The stability derivative of yawing force and yawing moment agree with the experimental results. The errors are 4.49% and 4.11%, respectively. The causes of errors may be that the supporting structure in the experiment is not included in the present study, which may have influence on the flow field.

4.1.2. Results for various drift angles

Fig. 8 shows the yawing moment varying with the drift angle. The red line is the computational values and the block points represent the experimental values. $N' = \frac{N}{0.5\rho V^2L^3}$, is the dimensionless yawing moment. $N'_v = -\frac{N'}{\cos\beta\sin\beta}$, is the stability derivative of yawing moment. $N'_v = -0.01153$, is got from the computational values and the experimental values is -0.011254 (Roddy, 1990), the error is 2.45%.

4.2. Simulations with the fully appended SUBOFF model

The SUBOFF with all appended model is also commuted, including the hull, sterns and the sail. There is also a ring wing in some documents about the experiments, but it is not considered in the present study.

4.2.1. Results for direct resistance

Numerical results of direct resistance with the fully appended SUBOFF are compared with the experimental values (Roddy, 1990) (as shown in Fig. 9). The maximum difference is 4.8%, which indicates that they are in good agreements with each other.

4.2.2. Results for various drift angles, pitch angles and angular velocities

The linear hydrodynamic coefficients are shown in Figs. 10–12. Y'_v and N'_v can be computed form Fig. 10. $Y'_v = -\frac{Y'}{\cos\beta\sin\beta}$, is the dimensionless yawing force varies with drift angles. $N'_v = -\frac{N'}{\cos\beta\sin\beta}$, is the dimensionless yawing moment varies with drift angles. Z'_w and M'_w can be computed form Fig. 11. $Z'_w = -\frac{Z'}{\cos\alpha\sin\alpha}$, is the dimensionless pitch force varies with pitch angles. $M'_w = -\frac{M'}{\cos\alpha\sin\alpha}$, is the dimensionless pitching moment varies with pitch angles. $Y'_r = \frac{Y/\Omega}{0.5\rho VL^3}$, is the stability derivatives of yawing force. $N'_r = \frac{N/\Omega}{0.5\rho VL^4}$, is the stability derivative of yawing moment, in which Y and N can be computed from Fig. 12. The comparisons between the computational values and experimental values are shown in Table3. Because we did not find the experimental data with exact the same model, we have to make approximate linear correction by $\phi_f = \phi_{f+R.W.} + \phi_{B.H.} - \phi_{B.H.+R.W.}$, where ϕ_f is the value for fully appended model in Table 3, $\phi_{f+R.W.}$ is the value for fully appended model plus a ring wing, $\phi_{B.H.}$ is the value for bare hull model, and $\phi_{B.H.+R.W.}$ is the value for bare hull model plus a ring wing, respectively. The influence of the ring wing is considered independent of other components. The relative errors are almost smaller than 10%. The difference for pitch force is relatively larger, because the experimental results demonstrate remarkable nonlinear characteristic as shown in Fig. 11 (a), in which the experimental and numerical results are almost parallel for the positive angles, but notably different for the negative angles.

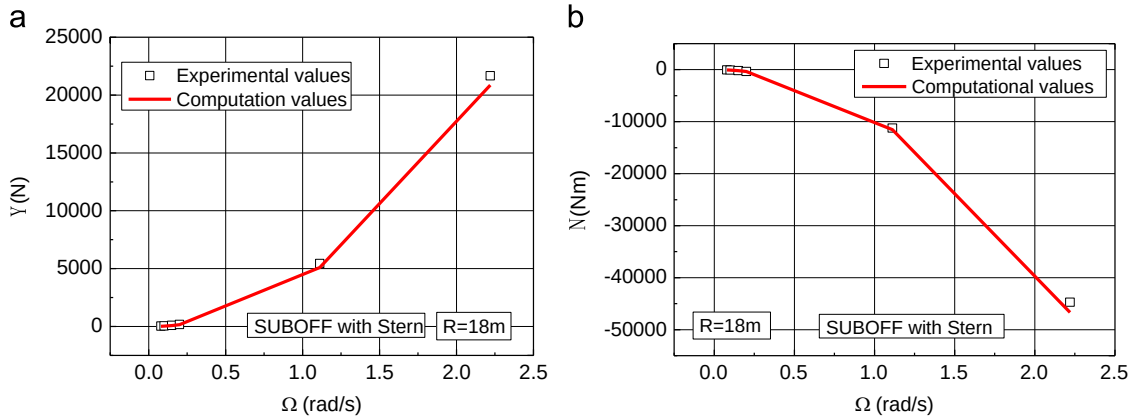

Fig. 7. (a) Yawing force vary with angular velocity (SUBOFF with sterns). (b) Yawing moment vary with angular velocity (SUBOFF with sterns).

Table 2
Stability derivatives of SUBOFF with sterns model.

Items	Computational values	Experimental values (Roddy, 1990)	Relative errors (%)
Y'_r	0.00604	0.006324	−4.49
N'_r	−0.00319	−0.003064	4.11

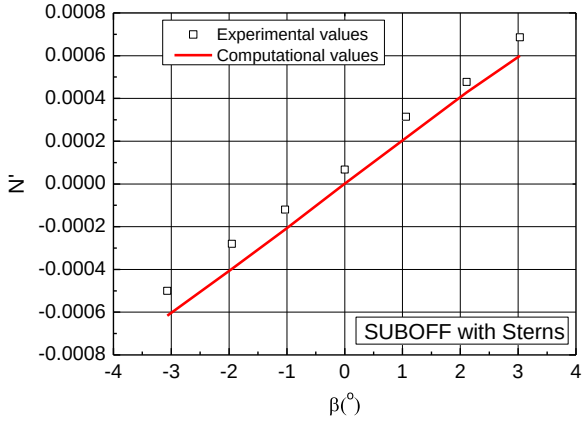

Fig. 8. Yawing moment varying with the drift angle (for the SUBOFF-sterns model).

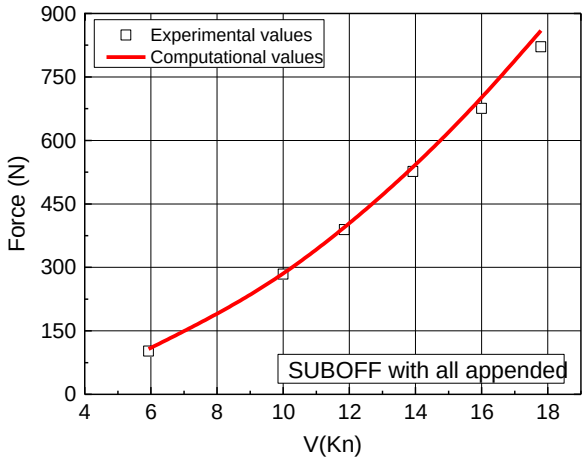

Fig. 9. The direct resistance varying with the speed (SUBOFF with all appended).

4.3. Discussions on the comparison between classic approaches and the present method

For the classic approach, the computation domain is similar to the rotating arm test pool and established on a body-fixed coordinate system (Zhang et al., 2013). Therefore, the outer flow moves in arc trajectories. The main purpose of changing the grid with different rotating radius is to make the boundary flow field parallel to the flow direction of the main flow, because it is important to avoid that both inflow and outflow regions exist in the same lateral boundary. Indeed this is not necessary to vary the grid for each simulation, but it is very beneficial to ensure the accuracy.

In the present approach, there are some differences by using the hybrid coordinate system, such as:

The outer computation domain is set in the absolute coordinate system. So, the main flows at different radiuses are parallel to a straight line. A straight boundary is aligned with the outer flow field.

The inner computation domain is set in the body-fixed coordinate system, which can improve the numerical predictions. So, the simulation results accuracy can be ensured without changing the mesh.

When the non-zero pitch and drift angle exists, the outer stream lines are still straight. If the mesh is not reconstructed, the lateral boundary is still identical as an inflow or outflow boundary. Therefore in this condition, the precision can still be ensured.

In the recent and state-of-the-art research paper by using RANS method of Zhang et al (2013), the authors change the grid for each simulating condition to ensure a body fitted structured grid aligned with the local flow field. The hydrodynamic force and moment coefficients for the SUBOFF-with-sting hull in steady turn with $Re = 6.5 \times 10^6$ were calculated. The differences of yawing force and moment coefficients between the experimental results and CFD results are about 6% and 5%, respectively, which mainly vary with the drift angle. However, in an individual condition that the drift angle is small ($\beta = 3.8^{\circ}$), the difference of yawing moment coefficients between experimental and CFD results is larger than 20%. In the present paper, the differences of the hydrodynamic force and moment coefficients of SUBOFF-stern model are less than 5%. The differences for fully appended model are around 9% which may cause by the distinctions of the model geometries. However, the difference is not only related with the CFD method strategy but also with the processing of experimental error or the mesh resolution and so on. It is believed that the precision is close to that in reference (Zhang et al., 2013). In consequence, the present approach is applicable for engineering designs and can achieve similar precision to the classic approaches.

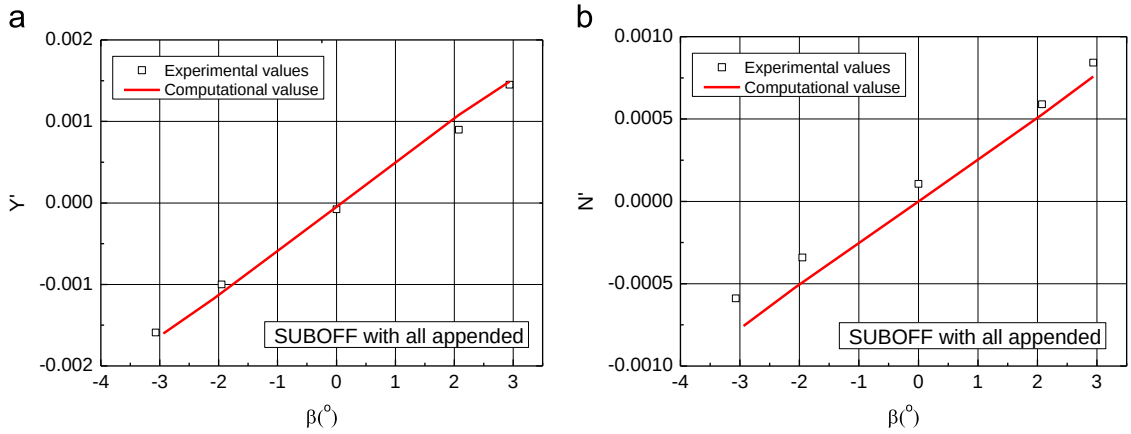

Fig. 10. (a) Yawing force varying with drift angle (SUBOFF with all appended). (b) Yawing moment varying with drift angle (SUBOFF with all appended).

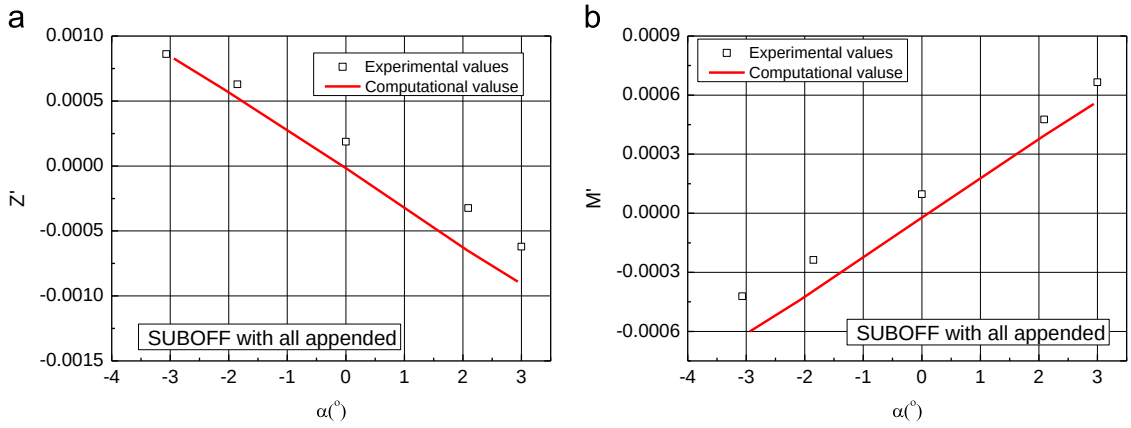

Fig. 11. (a) Pitch force varying with pitch angle (SUBOFF with all appended). (b) Pitching moment varying with pitch angle (SUBOFF with all appended).

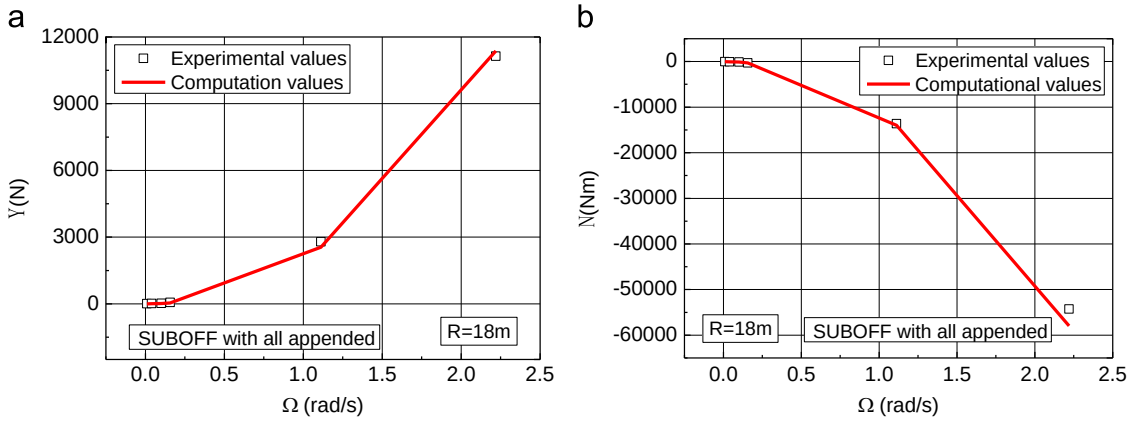

Fig. 12. (a) Yawing force varying with angular velocity (SUBOFF with all appended). (b) Yawing moment varying with angular velocity (SUBOFF with all appended).

5. Influence of controlling parameters

For the steady turning maneuverability simulation, the dimensional analysis method can be used to derive the control parameter. Using the yawing force as an example,

$$F = f(\rho, V, \Omega, D, \mu, \alpha, \beta) \tag{9}$$

where ρ is the density of the fluid, D is the diameter of the vehicle, V and Ω are the linear and angular velocities of the vehicle, μ is the dynamic viscosity, α is the pitch angle, β is the drift angle, respectively. Taking ρ, V, Das the dependent variables, the equation can be dimensionless as:

$$\frac{F}{1/2\rho V^2 L^2} = f(\Omega D/V, \mathrm{Re}, \alpha, \beta) = f'(R_0/D, \mathrm{Re}, \alpha, \beta) \tag{10}$$

R_0/D, is the ration between the radius of rotating arm tank and the diameter of the vehicle model, which represents a turning angular velocity in the dimensionless form. Re is the Reynolds number, which represents the ratio between the inertial effects and viscous effects. For the high speed underwater vehicle, the Reynolds number is usually greater than 10^6, which meets the self-simulation conditions. Therefore the effect of Reynolds number is negligible in most conditions. The flow similarity depends mainly on R_0/D, where R_0 is the radius of rotating arm tank. Flow similarity will be verified first in this section for fixed radius R_0, then

the influence of the angular velocity, Ω on the flow field are discussed with the same linear velocity, V. Finally influences of the pitch angle α and the drift angle β are investigated respectively.

5.1. Similarity of flow field when rotating radius Ω is fixed

The effect of angular velocity is calculated in this section with the fixed rotation radius. Figs. 13 and 14 show the wall friction and pressure contour distributions with different angle velocities. The trends of wall friction distributions are consistent with each other under different angle velocities, and the value of pressure coefficient is unchanged with the speed varying. All of these parameters can be used to verify the analysis of similarity above, and show that this method has a good accuracy for flow field simulation. In the Figs. 13 and 14, the flow patterns at $\Omega=0.1$ rad/s are slightly different from the others on the right regions around the sterns. This is because the Reynolds number is rather small under these conditions, which leads to a slightly enlarged separation zone downstream of the vertical sterns. This is similar to the mechanism of the classical flow around a circular cylinder, in which the laminar separation occurs before the turbulence separation.

5.2. The influence of rotating radius N'_r when linear velocity V is fixed

The influence of angular velocity Ω on the flow field is discussed with the same linear velocity V. The distributions of wall friction and pressure contour with different turning radius are shown in Figs. 15 and 16. As seen from the graphs, the trend of friction distribution appears obvious difference, and the value ranges of pressure coefficient maintain unchanged. With the increasing of angular velocity, the rotating radius becomes smaller, the rotation effect of flow field gradually increases, and the wake appears to have a significant left deflection. The separation zone in the left side of the vertical sterns is increasingly obvious (Figs. 15 and 16).

Table 3
Stability derivatives of SUBOFF with all appended.

Items	Computational values	Experimental values (Roddy, 1990)	Relative errors (%)
Y'_v	−0.03046	−0.027839	8.6
N'_v	−0.01470	−0.013504	8.9
Z'_w	−0.01685	−0.013915	21.0
M'_w	0.01135	0.010468	8.4
Y'_r	0.00339	0.003251	4.3
N'_r	−0.00400	−0.003716	7.6

5.3. The influence of pitch angle α

The influence of pitch angle α of the vehicle to the flow field is discussed with the same linear velocity V. The distribution of wall friction and pressure contour with different pitch angles α are shown in Figs. 17 and 18. When the pitch angle is negative, the flow streams move from the lower side to the upper side, so they gather at the downstream of the sail (as shown in the middle view of Fig. 17). Conversely when the pitch angle is positive, the flow streams spread out at the downstream of the sail (as shown in the right view of Fig. 17). The wake patterns appear asymmetric between top and bottom when the pitch angle is not zero. There are separation zones above horizontal sterns when the pitch angle is negative (as shown in the middle view of Fig. 18), and the pattern is approximately mirrored when the pitch angle is positive (as shown in the right view of Fig. 18)

5.4. The influence of drift angle β

The influence of drift angle β of the vehicle to the flow field is discussed with the same linear velocity$V$. As the existence of drift angle, the flow streams are oblique at the downstream of the sail (as shown in Fig. 19), and the wake patterns appear remarkably asymmetric between right and left (as shown in Fig. 20).

A comparison of vorticity magnitude distribution on cross-sectional planes is shown in Fig. 21. The vorticity distribution of the SUBOFF with sterns model are similar to the SUBOFF with all appended model. The crossflow separation effect along the tail is significant, and the wake of the sail has a certain effect on the flow around the top stern, inducing a detaching vortex at the downstream (as shown in Fig. 21).

6. Conclusions and discussions

The hybrid reference frame method, which combines the inertial and rotating reference frames with the added momentum source method, is proposed in this paper. A single mesh is needed for all conditions of a testing model, such as different rotating arm radius, pitch angles and drift angles.

By varying the angular velocity and the drift angle, stability derivatives of yawing moment and yawing force are obtained and meet well with the experimental results. The maximum errors of the SUBOFF-sterns model are limited within 5%, which shows that the present method is effective for engineering applications. The hydrodynamic coefficients for various drift angles, pitch angles and angular velocities with the fully appended SUBOFF models are also computed, and relative errors are almost smaller than 10%. By comparison with the classic method, it indicates that the present

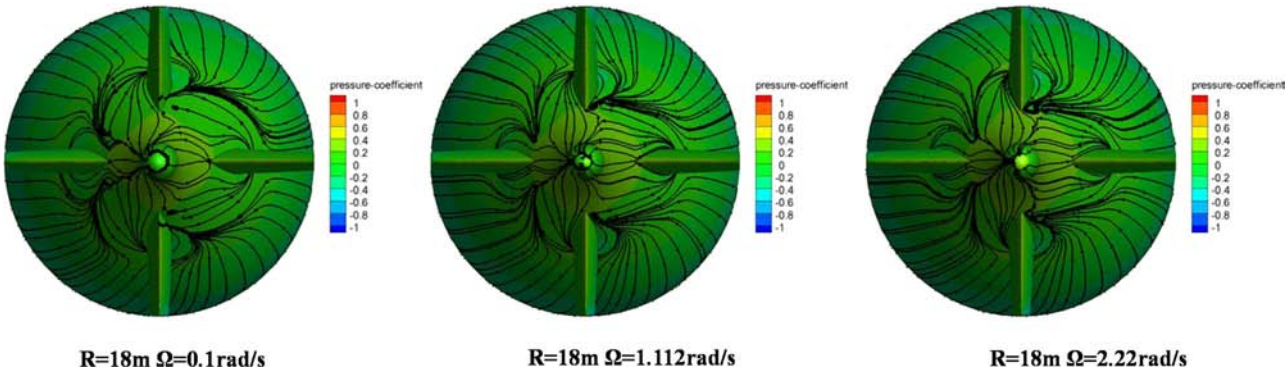

Fig. 13. Distributions of wall friction and pressure coefficient with different angular velocities (SUBOFF with sterns).

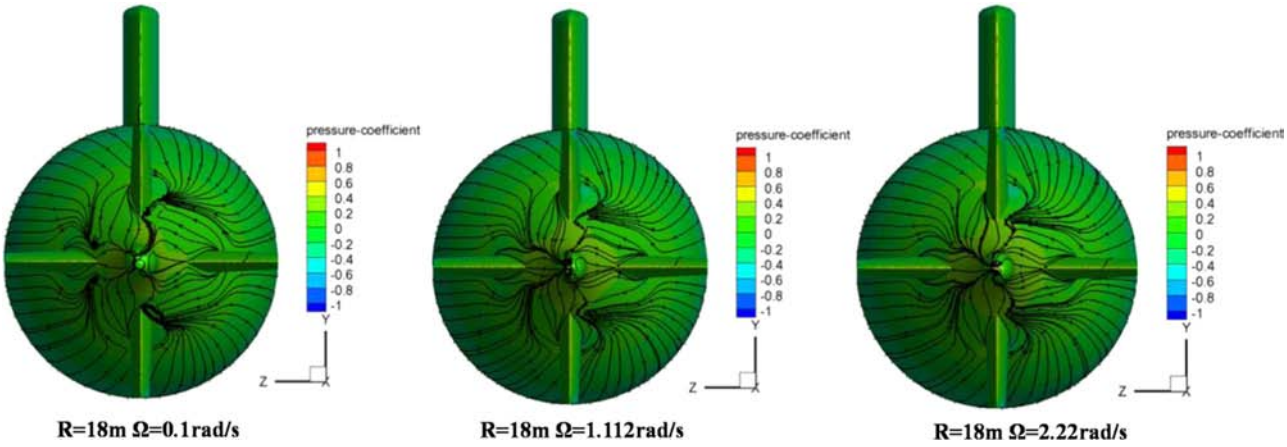

Fig. 14. Wall friction and pressure coefficient distribution with different angular velocity Ω (SUBOFF with all appended).

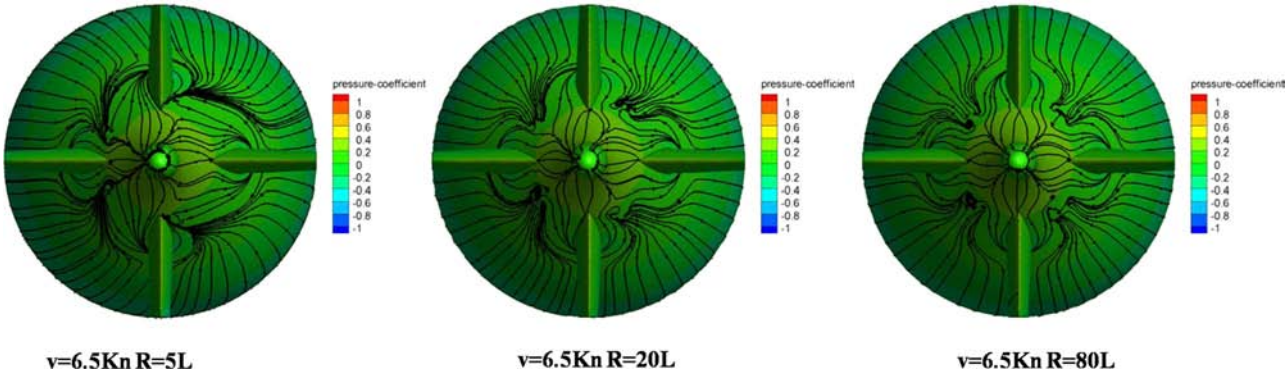

Fig. 15. Wall friction and pressure coefficient distribution with different R (SUBOFF with sterns).

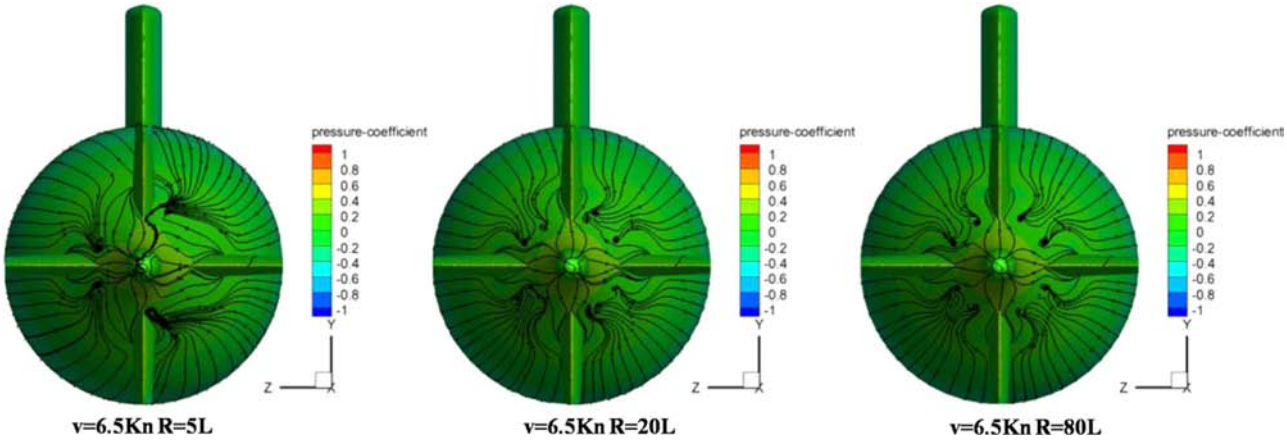

Fig. 16. Wall friction and pressure coefficient distribution with different R (SUBOFF with all appended).

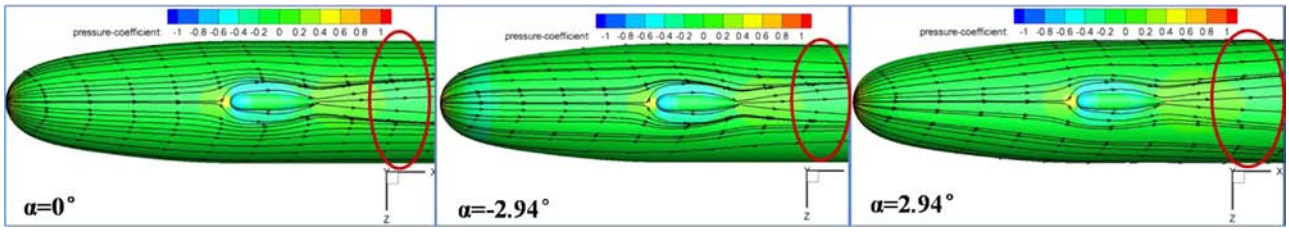

Fig. 17. Wall friction and pressure coefficient distribution with different pitch angle-around the sail (SUBOFF with all appended).

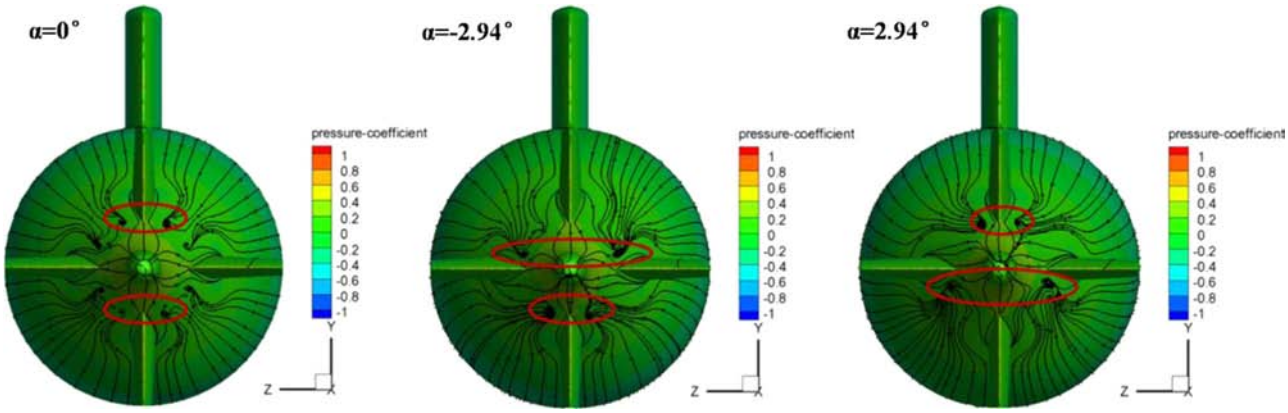

Fig. 18. Wall friction and pressure coefficient distribution with different pitch angle-around the sterns (SUBOFF with all appended).

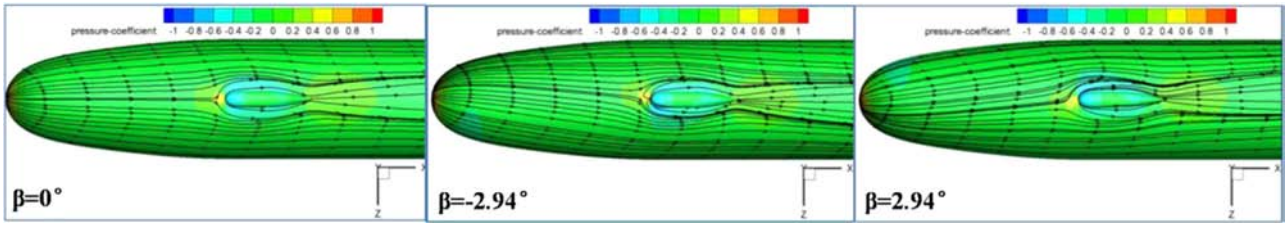

Fig. 19. Wall friction and pressure coefficient distribution with different drift angle-around the sail (SUBOFF with all appended).

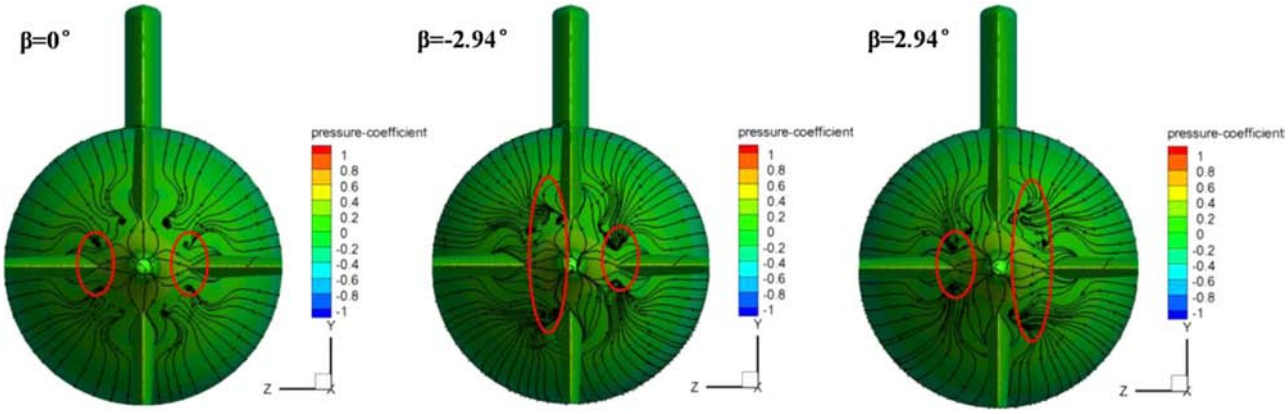

Fig. 20. Wall friction and pressure coefficient distribution with different drift angle-around the sterns (SUBOFF with all appended).

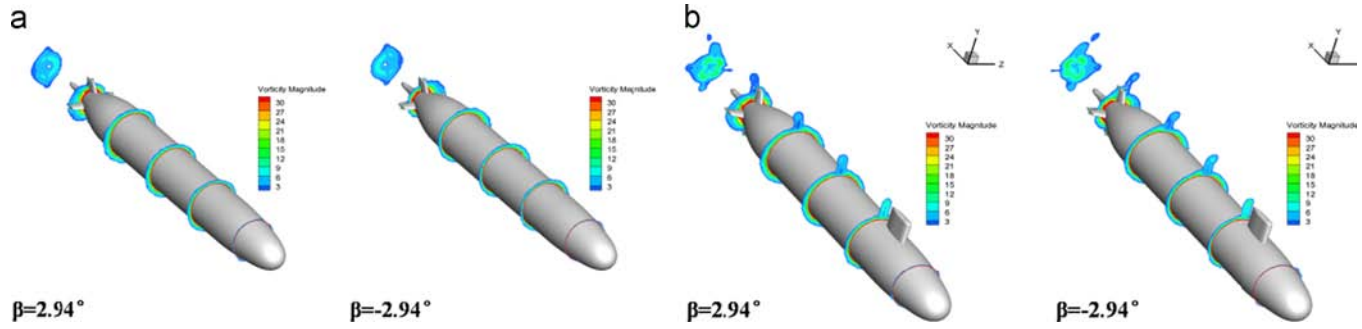

Fig. 21. (a) Vorticity magnitude on cross-sectional planes (SUBOFF with sterns). (b) Vorticity magnitude on cross-sectional planes (SUBOFF with all appended).

approach is applicable for engineering designs and can achieve similar precisions.

The influence of the rotating arm radius is also investigated. The computational results show that the similarity is consistent when the radius is constant, and the rotating effect is strong when the radius is small. The wake of the sail of the fully appended model has a certain effect on the flow around the top stern, inducing a detaching vortex at the downstream.

Acknowledgments

The authors are grateful to the Science and technology innovation project of Chinese Academy of Sciences through grant numbers KGFZD-125-014, National Natural Science Foundation of China through grant numbers 11202215, and the Youth Innovation Promotion Association of CAS (2015015).

References

Arabshahi, A., Gibeling, H.J., 2000. Numerical simulation of viscous flows about underwater vehicles. Oceans MTS/IEEE Conference. Vol. 3, 2000, 2185–2195.

Feldman, J., 1979. DTNSRDC revised standard submarine equations of motion. DTNSRDC/SPD-0393-09, June.

Gertler, M., Hagen, G.R., 1967. Standard equations of motion for submarine simulation. NSRDC Report 2510, June.

Gregory, P.A., Joubert, P.N., Chong, M.S., 2004. Flow over a body of revolution in a steady turn. DSTO-TR-1591.

Groves, N., Huang, T., Chang, M., 1989. Geometric Characteristics of DARPA SUBOFF Models (DTRC Models Nos. 5470 and 5471), DTRC Report SHD-1298-01, March.

Hess, D.E., Fu,T.C.Feldman, J.P., 2004. Naval maneuvering research and the need for shear stress measurements. In: Proceedings of the 24th AIAA aerodynamics measurement technology and ground testing conference. AIAA Paper 2004–2605, Portland; June.

Hu, Z.Q., Lin, Y., Gu, H.T., 2007. On numerical computation of viscous hydrodynamics of unmanned underwater vehicle. J. Robot Vol 29 (No 2), 145–150.

Hu, Z.Q., Lin, Y., 2008. Computing the hydrodynamic coefficients of underwater vehicles based on added momentum sources. In: Proceedings 18th International Offshore and Polar Engineering Conference. Vancouver, BC, Canada.

Huang, T., Liu, H.L., Groves, N., 1989. Experiments of the DARPA SUBOFF Program. DTRC Report SHD-1298-02, December.

Kim, K., Sutoh, T., Ura, T., Obara, T., 2001. Obara. Route keeping control of AUV under current by using dynamics model via CFD analysis Oceans. MTS/IEEE Conference, Vol 1, 2001, 417–422.

Mackay, M., 1999. Predicting the effect of a hull plug on submarine manoeuvring using semiempirical methods. JRINA International Symposium on Naval Submarines 6 (Warship' 99), London, June.

Mackay, M., 2009. DSSP50 build 090910 Documentation, Part 3: Algorithm Description. DRDC Atlantic TM 2009-228, December.

Orihara, H., Miyata, H., 2003. Evaluation of added resistance in regular incident waves by computational fluid dynamics: motion simulation using an overlapping grid system. J. Mar. Sci. Technol. Vol 8, 47–60.

Racine, B.J., Paterson, E.G., 2005. CFD-based method for simulation of marine-vehicle maneuvering. 35th AIAA Fluid Dynamics Conf, Toronto, Canada, AIAA 2005-4904.

Roddy, R. F., 1990. Investigation of the stability and control characteristics of several configurations of the DARPA SUBOFF model (DTRC MODEL 5470) from captive model experiments, 1990, David Taylor Research Center.Ship Hydromechanics Department Departmental Report.

Simonsen, C.D., Stern, F., 2005. RANS maneuvering simulation of Esso Osaka with rudder and a body-force propeller. J. Ship Res. 49 (2), 98–120.

Suzuki, H., Kato, N., Katayama, T., Fukui, Y., 2007. Motion simulation of an underwater vehicle with mechanical pectoral fins using a CFD-based motion simulator. Proceedings of International Symposium on Underwater Technology, pp. 384–390.

Watt, G.D., Nguyen, V.D., Cooper, K.R., Tanguay, B., 1993. Wind tunnel investigations of submarine hydrodynamics. Can. Aeronaut. Space J. 39 (3), 119–126.

Watt, G.D., Bohlmann, H.J., 2004. Submarine rising stability: quasi-steady theory and unsteady effects. In: Proceedings of the 25th Symposium on Naval Hydrodynamics, St. John's, August.

Wilcox, D.C., 2001. Turbulence Modeling: an Overview. In: Proceedings 39th Aerospace Science Meeting, Reno, America, A01-16558.

Williams, C.D., Mackay, M., Muselet, C., Perron, C., 2002. Physical modelling of vehicle performance in high-amplitude and high-rate manoeuvres. NATORTO SCI-120 Meeting, Berlin, May.

Zhang, J.T., Maxwell, J.A., Gerberet, A.G., 2013. Simulation of the flow over axisymmetric submarine hulls in steady turning. Ocean Eng. 57, 180–196.